Supersonic flow bifurcation in twin intake models

Alexander Kuzmin[*] and Konstantin Babarykin[a]

Department of Fluid Dynamics, St. Petersburg State University, 28 University Avenue, 198504, Russia

Abstract. Turbulent airflow in channels of rectangular cross section with symmetric centerbodies is studied numerically. Shock wave configurations formed in the channel and in front of the entrance are examined. Solutions of the unsteady Reynolds-averaged Navier-Stokes equations are obtained with finite-volume solvers of second-order accuracy. The solutions demonstrate an expulsion/swallowing of the shocks with variations of the free-stream Mach number or angle of attack. Effects of the centerbody length and thickness on the shock wave stability and flow bifurcation are examined. Bands of the Mach number and angle of attack, in which there exist non-unique flow fields, are identified.

Keywords: supersonic intake; shock waves; instability; hysteresis

1. Introduction

Studies of airflow in supersonic intakes are of practical interest in view of their importance for the efficient operation of aircraft engines. A mixed-compression intake consists of a convergent part, which lies upstream of the throat section and a divergent part downstream of the throat. In the design regime of operation there is a train of oblique shocks in the convergent part of the intake, where the flow is supersonic and a terminal shock downstream of the throat (Sforza 2012). For low contraction inlets, the design regime can be started by increasing the free-stream Mach number M_∞ up to a value that exceeds a Kantrowitz limit M_{start} (Kantrowitz and Donaldson 1945). If after that M_∞ turns to decrease, then the terminal shock moves upstream and, at some value $M_{unstart} < M_{start}$, it jumps out from the intake while the flow velocity drops to subsonic values.

The possibility of a hysteresis and flow bifurcation in the band $M_{unstart} < M_\infty < M_{start}$ was shown in classical works based on quasi-one-dimensional equations governing mass flow rate and stagnation temperature across the shock (Daneshyar 1976, Hill and Peterson 1992). In the last decade, the hysteresis of intake start/unstart was studied both numerically and experimentally. For a Busemann supersonic biplane, numerical simulations showed that the width $M_{start} - M_{unstart}$ of Mach number band, in which flow bifurcation occurs, is 0.54 (Kusunose *et al.* 2011, Hu *et al.* 2011). Subsequent experiments revealed some discrepancy between 2D numerical simulations and tests for 3D biplane models (Yamashita *et al.* 2013) which demonstrated the biplane start at lower

---

*Corresponding author, Professor, E-mail: a.kuzmin@spbu.ru
[a]Researcher, Ph.D., E-mail: konst20@mail.ru

<div align="center">(a)   (b)</div>

Fig. 1 Twin intakes used in jets: (a) North American $XB-70$ Valkyrie (Wikipedia 2017), (b) Russian TU-160 Blackjack (Военное обозрение 2018)

Mach numbers than those predicted by 2D computations.

Hypersonic intake start for high contraction ratios was investigated in (Chang *et al.* 2009, Timofeev and Mölder 2011, Mölder and Timofeev 2011), where a flow hysteresis under variations of the throat section and other geometry parameters was calculated at free-stream Mach numbers larger than 3.

Li *et al.* (2011) tested various flow characteristics in the intake starting process by using a high speed Schlieren system. Contraction ratio limits for the self-start were obtained and the leading edge bluntness was shown to play an important role in the process.

Ben-Dor (2015) presented a review of recent studies of flow hysteresis in the regular/Mach shock reflection from a wall and noticed that some of the explored geometries were similar to ones of intakes. The reflections admit up to three different flow regimes at the same free-stream parameters (Ben-Dor 2007). This must be taken into account in supersonic and hypersonic vehicles design, as different flow fields in the same flight conditions may essentially influence the fuel combustion and aerodynamic performance of the flying vehicle.

The start/unstart transitions in a hypersonic intake were also investigated by Jiao *et al.* (2015, 2016) who revealed that the interaction of external compression shocks and boundary layer on the cowl plays a key role in the hysteresis phenomenon induced by variation of the cowl angle or downstream pressure. Xu *et al.* (2016) and Chang *et al.* (2017) presented recent studies of unstart mechanisms, monitoring methods and methods for unstart suppression and control. Tao *et al.* (2008, 2009) analyzed the hypersonic intake start/unstart using topological methods and Thom's catastrophe theory.

Transonic flow in simple geometries, modeling intakes of rectangular cross section was examined by Kuzmin (2016). Shock wave bifurcations were studied for a few locations of the throat, cowl deflection angles and $1.3 \leq M_\infty \leq 1.73$. Numerical solutions revealed jumps of the shock leg position and considerable hysteresis under variations of M_∞. Ryabinin and Suleymanov (2016) explored the supersonic flow in a symmetric 2D channel of variable cross-section with a centerbody located downstream of the entrance. Numerical simulations showed the existence of a flow hysteresis in a band of the inlet Mach number.

Kuzmin and Babarykin (2016) studied numerically 2D and 3D turbulent airflow in convergent-

divergent symmetric channels with a centerbody whose profile is a double wedge, or thin plate, or smooth circular-arc airfoil. The formation of diverse flow regimes at supersonic free stream velocities and vanishing angle of attack were discussed. Special attention was paid to steady asymmetric flows in which there exists a train of oblique shocks on one side of the centerbody, whereas an expelled shock forms on another side.

In the present paper we perform further study of the turbulent transonic flow in channels of rectangular cross section. Both centerbodies and channels are symmetric about the planes $y=0$ and $z=0$; they may be treated as simple models of twin intakes used in some aircraft, see Fig. 1. In Sections 2 and 3 we formulate the problem and outline a numerical method. In Section 4, we study a dependence of 2D flow bifurcation on the Mach number and angle of attack for 12% and 10%-thick centerbodies. For simplicity, we consider a channel whose exit is opened to the external flow; this condition yields the supersonic flow regime at the exit. An influence of 3D effects on the flow is examined in Section 5. Finally, a dependence of the flow on the centerbody length and its slope downstream of the throat is studied in Section 6. Again, we impose the supersonic flow condition at the channel exit and do not treat regimes admitting interactions with other engine components.

2. Formulation of the problem

Let profiles of the upper and lower walls of the channel be thin rectangles parallel to the x-axis

$$0.25 \leq y \leq 0.252, \quad -0.252 \leq y \leq -0.25, \quad \text{where} \quad x_1 \leq x \leq x_2 \tag{1}$$

see Fig. 2. Endpoints x_1 and x_2 are specified below in Sections 4 and 6. Here and further in the paper, the Cartesian coordinates (x, y, z) are dimensional and given in meters, except for Figs. 3 and 7 where we use millimeters for another channel.

In Sections 4 and 5, the profile of the centerbody is a rhombus of length 1 with vertices

$$x=\pm 0.5, \quad y=0 \quad \text{and} \quad x=0, \quad y=\pm T/2 \tag{2}$$

where T is the rhombus thickness (Fig. 2). A longer centerbody will be treated in Section 6.

The inlet boundary of the computational domain is set at $x= -0.75$, $-2 \leq y \leq 2$. The outlet boundary is $x=0.8$, $-2 \leq y \leq 2$. The upper and lower boundaries are remote at $y=\pm 2$ in order to eliminate their interaction with bow shock waves produced by the walls. The x-, y- and z-components of the flow velocity on the left boundary of the computational domain are

$$U_\infty = M_\infty a_\infty \cos \alpha, \quad V_\infty = M_\infty a_\infty \sin \alpha, \quad W_\infty = 0 \quad \text{at} \quad x=-0.75, \quad -2 \leq y \leq 2 \tag{3}$$

where $M_\infty > 1$ and α is the angle of attack. Also we prescribe on the left boundary the static pressure $p_\infty = 10^5$ N/m^2, a turbulence level of 0.2% and static temperature $T_\infty = 250$ K which determines the sound speed $a_\infty = 317.02$ m/s. The outlet is endowed with a condition of the supersonic flow regime. The no-slip condition and vanishing heat flux are imposed on the walls and centerbody. A free-slip condition is used on the upper and lower boundaries of the computational domain. Initial data are either parameters of the free stream or a flow field calculated for a different free-stream Mach number. The air is treated as a perfect gas whose specific heat at constant pressure is 1004.4 J/(kg K) and the ratio of specific heats is 1.4. We adopt the value of 28.96 kg/kmol for the molar mass and use the Sutherland formula for the molecular dynamic viscosity. Free-stream Mach numbers under consideration lie in the range $1.6 \leq M_\infty \leq 2.2$; therefore, the Reynolds number based on the middle of the range and length of 1 m is 4.4×10^7.
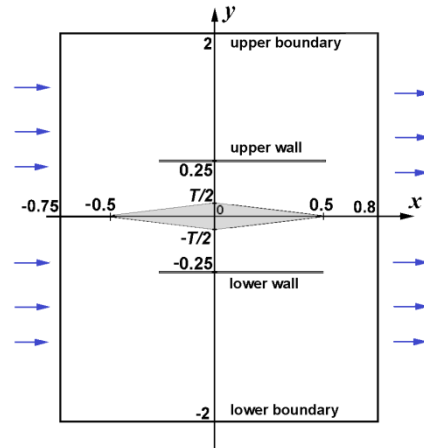
Fig. 2 Schematic of the computational domain

(a)   (b)
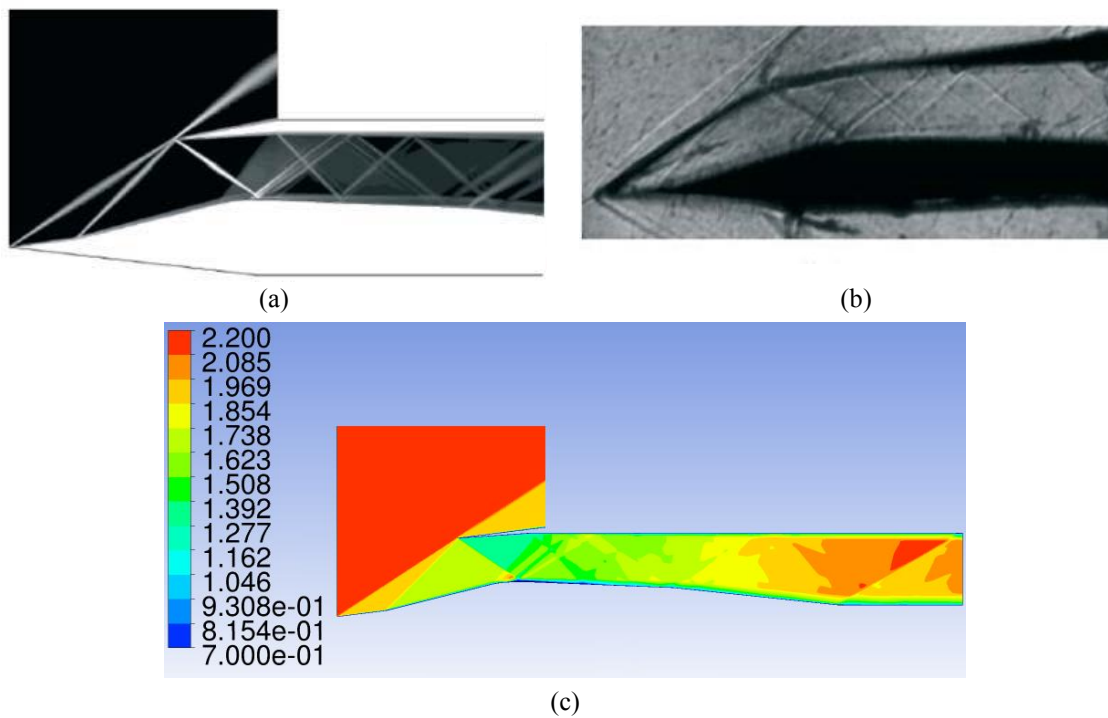

(c)

Fig. 3 An intake used for the solver validation. Mach number contours at M_∞=2.2 and cowl deflection angle of 4 deg: (a) and (b) numerical simulations and experimental data, respectively, reproduced from (Das and Prasad 2010) with permission; (c) our computations with ANSYS-15 CFX. The length of the channel displayed in (c) is 119 mm

3. A numerical method

Solutions of the unsteady Reynolds-averaged Navier-Stokes equations were obtained with

ANSYS-15 CFX finite-volume solver of second-order accuracy in space and time. The solver is based on a high-resolution discretization scheme by Barth and Jespersen (1989) for convective terms. An implicit backward Euler scheme is employed for the accurate time-stepping. The code employs a linearization of the discretized equations and a multigrid accelerated factorization technique for solving the system of linear equations. In addition, a few simulations were performed with ANSYS-15 Fluent density-based solver (see Fig. 6). We used a Shear Stress Transport k-ω turbulence model, which is known to reasonably predict aerodynamic flows with boundary layer separations (Menter 2009).

2D computational meshes were constituted by quadrangles in 37 layers on the walls and centerbody and by triangles in the remaining region. The non-dimensional thickness y^+ of the first mesh layer was less than 1. Test computations on uniformly refined meshes of approximately 2×10^5, 6×10^5 and 18×10^5 cells showed that a discrepancy between shock wave coordinates obtained on the second and third meshes did not exceed 1%. Global time steps of 5×10^{-7} s and 10^{-6} s yielded indistinguishable solutions. For this reason, the time step of 10^{-6} s and meshes of 6×10^5 cells were employed in the study of 2D transonic flow at various Mach numbers. The root-mean-square CFL number (over mesh cells) was about 2.

3D flow simulations were carried out for a channel created by an extrusion of the 2D profile from $z=0$ to $z=0.15$ or 0.30. Details of the 3D problem formulation are given in Sections 5 and 6.

The solver was validated by computation of several benchmark transonic flows (Kuzmin 2014, 2016). In addition, we recomputed supersonic flow in an intake suggested by Das and Prasad (2010) and found good agreement with their calculations and experiments, see Fig. 3.

4. 2D flow simulations for the centerbody length of 1

First, we addressed the symmetric flow over the centerbody of thickness $T=0.12$ in the channel with walls (1) which extend from $x_1 = -0.25$ to $x_2 = 0.5$. The uniform free stream (3) was used for initialization of the solution. Computations showed a convergence of the mean parameters of turbulent flow to a steady state in less than 0.2 s of physical time. At $\alpha=0$ and $M_\infty=1.65$, the flow field exhibits oblique shocks generated by the centerbody and nearly normal shocks in front of the entrance. As seen from Fig. 4(a), interaction of the shocks creates a flow pattern with triple points and boundary-layer separation. If M_∞ increases step-by-step from 1.65 to 1.8 (so that the calculated steady flow at each step is used as initial data for the next M_∞), then the shock system shifts downstream and eventually enters the channel. Further increase of M_∞ to the band $1.87 \leq M_\infty \leq 1.91$ results in formation of a supersonic bridge over the separated boundary layer on both sides of the centerbody, see Fig. 4(b). The bridge connects the supersonic regions located upstream of the entrance and downstream of the throat. If M_∞ exceeds the value of 1.91, then computations show a jump of the shock system downstream, a boundary-layer reattachment and relaxation to the flow pattern with a train of oblique shocks (Fig. 4(c)).

The qualitative flow pattern with the train of shocks persists when M_∞ turns to decrease step-by-step from 1.92 to 1.88 and then to 1.70, yielding a gradual shift of the shocks upstream. Further decrease of M_∞ to 1.69 results in an abrupt expulsion of the shocks from the channel and transition to the flow field with shock waves located in front of the entrance. Therefore, in the band
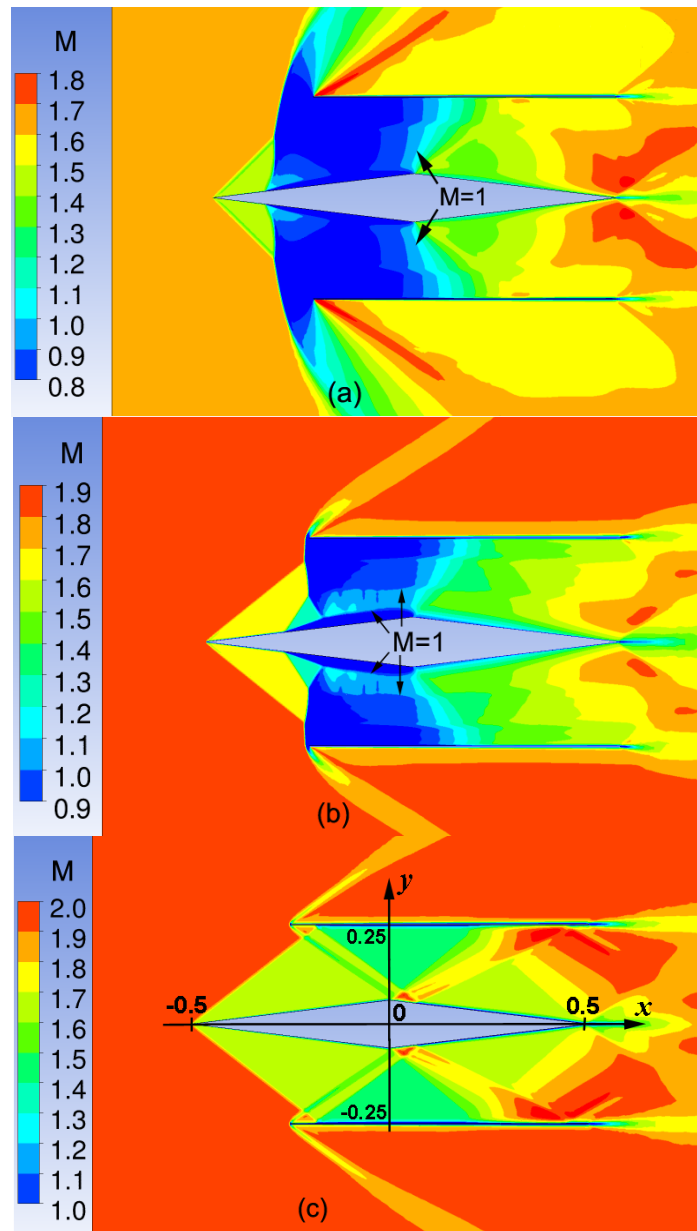
$$1.70 \leq M_\infty \leq 1.91 \tag{4}$$

Fig. 4 Mach number contours in symmetric 2D flow at the vanishing angle of attack α=0: (a) M_∞=1.65, (b) M_∞=1.88; the solution is obtained by increasing M_∞ from 1.65 to 1.88, (c) M_∞=1.92

there exist two different symmetric flow regimes: one with expelled shocks and another with a train of shocks in the channel. The realization of a certain regime depends on the time history of M_∞. A physical interpretation of the hysteresis is the same as for convergent-divergent channels without centerbodies, i.e., its origin is the existence of two different flows in the same band of M_∞, as considerations of the mass flow rate and non-isentropic relations across a normal shock show (Hill and Peterson 1992).
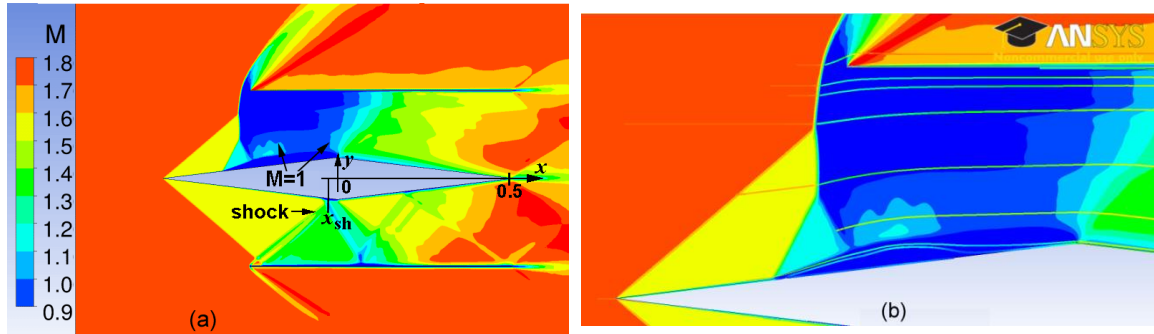
Fig. 5 Asymmetric 2D flow with an expelled shock in the upper part of the channel and a train of shocks in the lower part, $M_\infty=1.8$, $\alpha=0$: (a) Mach number contours; (b) streamlines in the region of boundary-layer separation

To obtain at $\alpha=0$ an asymmetric flow over the symmetric centerbody, we first solved the problem for the piecewise constant free-stream Mach number: $M_\infty=1.6$ at $0<y\leq2$, $M_\infty=1.8$ at $-2\leq y\leq0$ in (3). The solution exhibited an expelled shock above the centerbody and a swallowed shock system below it. Then a gradual increase of M_∞ at $y>0$ to the value of 1.8 yields the asymmetric flow pattern for $M_\infty=1.8$ at $-2\leq y\leq2$, see Fig. 5. The wavy shape of the sonic line above the centerbody in the entrance region is explained by multiple reflections of compression waves from the sonic line and separated boundary layer. In Fig. 5, the shape of Mach number contour $M(x,y)=0.9$ resembles two steps and hints at contact discontinuities emanating from the triple points. Though the separation bubble is large, there is no buffet onset in the flow conditions at hand.

The obtained asymmetric flow at $\alpha=0$ persists when M_∞ varies in the band

$$1.77 \leq M_\infty \leq 1.91 \qquad (5)$$

Another asymmetric flow in this band can be obtained by reflection of the flow field shown in Fig. 5 about the x-axis. Owing to (4), in the band (5) there exist two symmetric and two asymmetric flow regimes. We notice that an initialization of an asymmetric solution at $\alpha=0$ can also be performed by variations of α at a constant (not piecewise-constant) M_∞. This follows from a discussion of curves 1 presented in Fig. 6 below.

If M_∞ leaves the band (5), i.e., it exceeds 1.91 or falls below 1.77, then computations demonstrate a transition from the asymmetric flow to a symmetric one with swallowed or expelled shocks, respectively.

To trace streamwise positions of the bow shock generated by the lower wall of channel, we denote by x_{sh} the abscissa of its intersection with the centerbody (Fig. 5(a)) or abscissa of the triple point if the boundary layer separation occurs. Figure 6 shows dependencies of x_{sh} on the angle of attack calculated for $M_\infty=1.85$ and $M_\infty=1.95$. The upper branches of the curves correspond to flow regimes with swallowed shocks and the lower branches correspond to flows with swallowed shocks above the centerbody and expelled ones below it. As seen, the results obtained with ANSYS-15 CFX and Fluent solvers are in reasonable agreement.

A smoothing of the rhombus (2) at the vertices $x=0$, $y=\pm0.06$ with circular arcs of the radius of 0.2 influences the flow insignificantly. In this case the band (5) admitting asymmetric flow at $\alpha=0$ slightly expands to $1.77 \leq M_\infty \leq 1.92$.
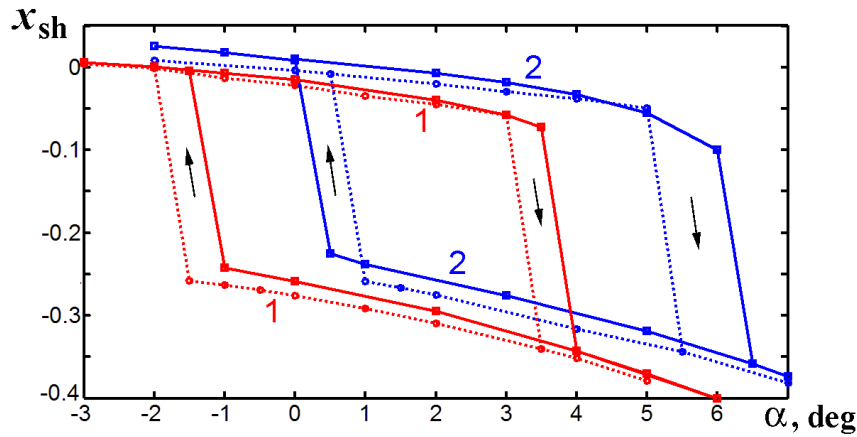
Fig. 6 Coordinate x_{sh} of a shock wave generated by the bow of the lower wall versus the angle of attack α. Curves 1: M_{∞}=1.85, curves 2: M_{∞}=1.95. Solid curves – computations with ANSYS-15 CFX, dashed curves – computations with ANSYS-15 Fluent density-based solver
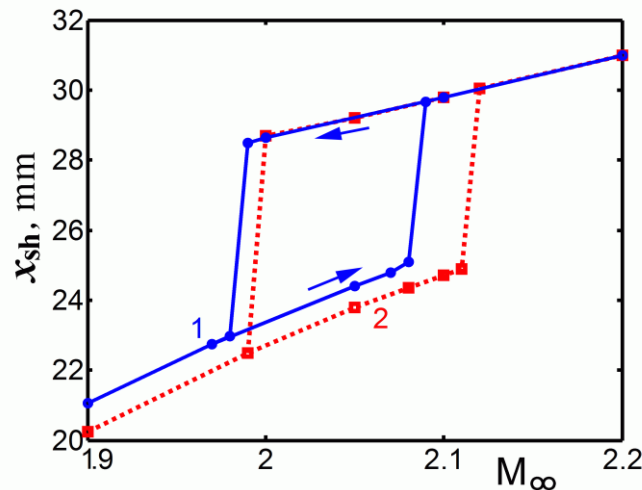

Fig. 7 Coordinate x_{sh} of the oblique shock at the height of 9.5 mm in the intake shown in Fig. 3: 1 – original intake (Das and Prasad 2010) with the smoothed lower wall at the throat; 2 – modified intake with a corner of the lower wall profile at the throat

We notice that the use of a Baseline Reynolds stress turbulence model instead of the SST $k-\omega$ one yields just a minor effect on the shock location and hysteresis (Kuzmin 2015, 2016). Also, computations reveal negligible distinctions between flow fields obtained for the perfectly smooth walls/centerbody and rough ones with a sand-grain roughness of 10^{-5} m.

Flow simulations for a halved pressure, p_{∞}=5×10^4 N/m^2 and therefore halved Reynolds number, showed that the band (5) of asymmetric flow regimes at α=0 slightly shifts to larger values of M_{∞}: $1.77 \leq M_{\infty} \leq 1.935$.

For the reduced centerbody thickness, T=0.1 in (2) and coordinates $x_1 = -0.3$, $x_2 = 0.5$ of the beginning and end of walls in (1), the band of asymmetric regimes at α=0 shifts to smaller Mach

numbers: $1.68 \leq M_\infty \leq 1.82$.

It is worth mentioning that flow simulation in the intake depicted in Fig. 3 also reveals a shock position hysteresis. The hysteresis takes place at $1.99 \leq M_\infty \leq 2.08$, see curve 1 in Fig. 7. Here x_{sh} is the abscissa of an intersection of the oblique shock reflected from the cowl with a horizontal line $y=9.5$ mm located above the boundary layer. If the smoothing of the lower wall near throat (Das and Prasad 2010) is replaced by a corner created by prolongations of profile segments, then the hysteresis band slightly expands: $2.00 \leq M_\infty \leq 2.11$, see curve 2 in Fig. 7.

5. 3D flow simulations for the centerbody length of 1

Now we turn to a 3D channel created by an extrusion of the 12%-thick centerbody and walls with $x_1 = -0.25$, $x_2 = 0.5$ from the plane $z=0$ to $z=\pm0.3$. For CPU savings, we suppose the flow to be symmetric about the plane $z=0$; this makes it possible to calculate the flow only in a half of the domain, e.g., at $z>0$. The inner and outer surfaces of the sidewall are located in the planes $z=0.3$ and $z=0.302$, respectively. The side boundary $z=1.4$ of the computational domain was endowed with the free-slip condition. A mesh sensitivity study was performed using three-dimensional meshes up to 17×10^6 hexahedrons with refinement in the boundary layers to meet the condition $y^+<1$.

Figure 8 displays shock waves and isosurfaces $M(x,y,z)=1.7$ at $M_\infty=1.8$. As seen, the streamwise location of shocks is similar to that in 2D flow (Fig. 5). This is confirmed by Mach number distribution in the plane of symmetry, see Fig. 9(a). Meanwhile, Mach number contours in the plane $z=0.15$ differ noticeably from those in the plane of symmetry (cf. Figs. 9(a) and 9(b)). Distinctions become especially evident in the plane $z=0.25$ located near the side wall where an essential boundary layer separation develops (Fig. 9(c)).

Figures 10(a) and 10(b) display Mach number contours in cross sections $x=0.1$, -0.15, -0.35. As seen, the flow structure near the sidewall looks like a fin-type configuration or corner flow (Nguyen *et al*. 2011) in which the ramp shock interacts with the weak shock produced by the sidewall and impinges on the boundary layer that is developing on the adjacent surface.

For a 3D channel of halved span, with the sidewall at $0.15<z<0.152$, a general view of the flow (Fig. 11) is similar to the one discussed in the previous case, though an impact of the sidewall is more pronounced. Figure 12 shows that even in the plane of symmetry $z=0$, which is at the maximum distance from sidewall, the flow field is different from 2D flow displayed in Fig. 5.

Thus, 3D flow computations confirm the existence of axisymmetric flow regimes at the vanishing angle of attack due to a weak correlation between flow fields beneath and above the centerbody in conditions under consideration.

6. 3D flow simulations for the centerbody length of 1

Finally, we consider a centerbody and channel extended downstream to the outlet boundary $x=0.8$. The rear part of rhombus (2) is replaced here by segments with endpoints $x=0$, $y=\pm0.06$ and $x=0.8$, $y=\pm0.036$. That is why the slope of the rear part is reduced from 6.84 deg to 1.72 deg. As a consequence, the divergence of centerbody and walls at $x>0$ is reduced and calculated Mach numbers downstream of the throat are decreased (cf. Figs. 13 and 5). The band (5), in which asymmetric flows at the vanishing angle of attack exist, slightly expands
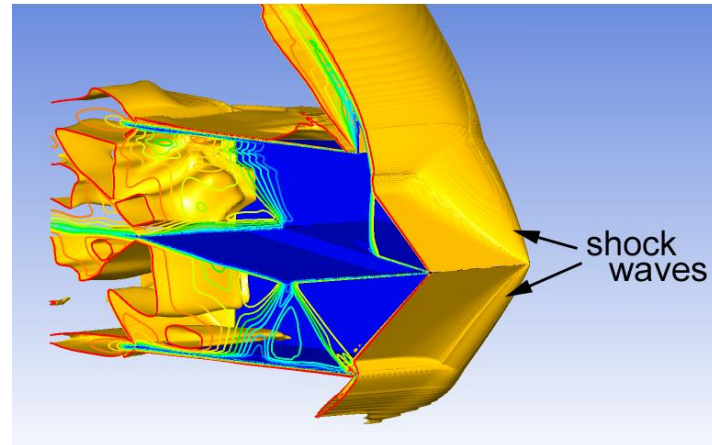
Fig. 8 Mach number contours in the plane *z*=0 and isosurfaces *M*(*x*, *y*, *z*)=1.7 over the 3D centerbody and channel of half-span 0<*z*<0.3. The same asymmetric flow regime at M_∞=1.8, α=0 as in Fig. 5
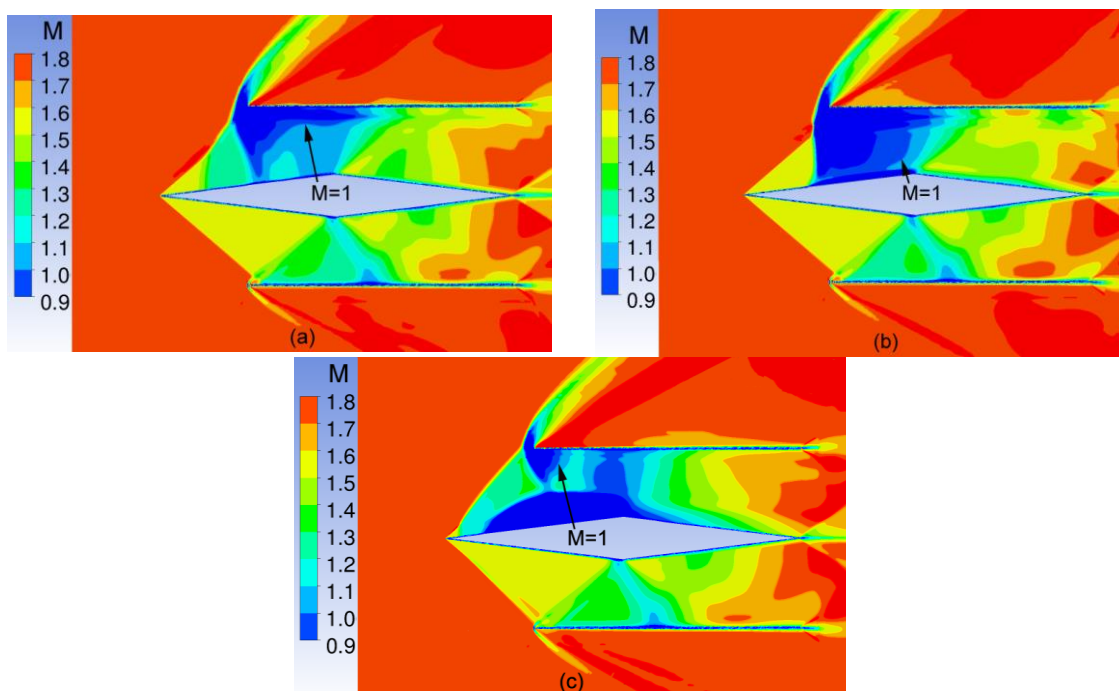

Fig. 9 Mach number contours in span sections of the 3D flow shown in Fig. 8: (a) *z*=0, (b) *z*=0.15, (c) *z*=0.25

$$1.76 \leq M_\infty \leq 1.94 \tag{6}$$

An increase of the upper bound is explained by a smaller flow acceleration at the throat because of the smaller divergence of channel at *x*>0. As a consequence, one needs a larger M_∞ to trigger the swallowing of shocks and transition to the symmetric state.

3D flow simulations were performed for the same half-span of the channel 0<*z*<0.3 as in Fig. 8. Again, we used the assumption of flow symmetry about the plane *z*=0. As seen from Fig. 14, the
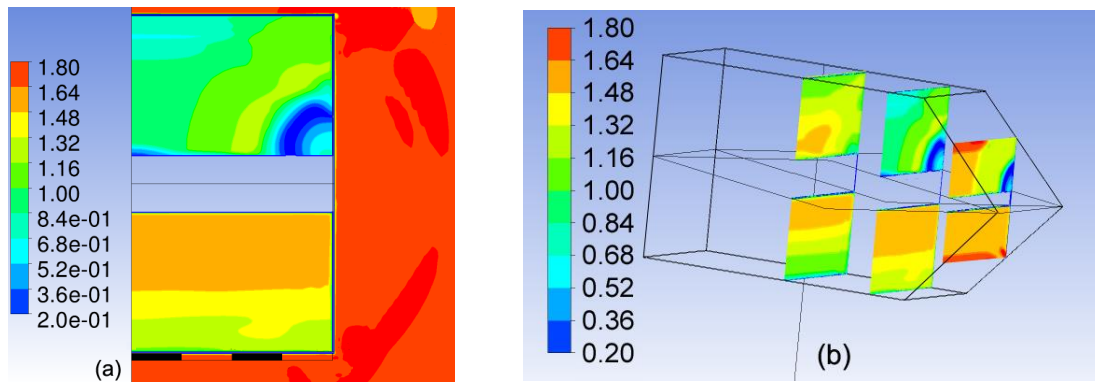
Fig. 10 Mach number contours in cross sections of the 3D flow shown in Fig. 8: (a) $x= -0.15$, (b) $x= 0.1$, -0.15, -0.35
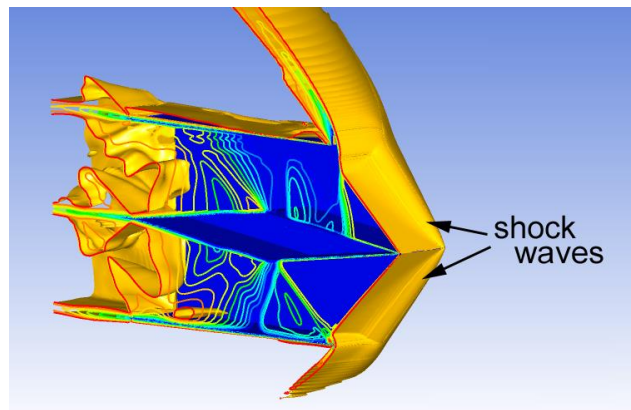

Fig. 11 Mach number contours in the plane $z=0$ and isosurfaces $M(x, y, z)=1.7$ over the 3D centerbody and channel of the reduced half-span $0<z<0.15$. The same asymmetric flow regime at $M_\infty=1.8$, $\alpha=0$ as in Fig. 5

flow behavior in the convergent part of the channel is the same as that in Fig. 8. Meanwhile, downstream of the throat, flow Mach numbers are smaller than in Fig. 8 because of the smaller cross sectional areas.

7. Conclusions

For the considered geometries of the centerbody and channel, numerical simulations of 2D turbulent flows demonstrated the occurrence of shock system instability with gradual variation of the free-stream Mach number M_∞ or angle of attack α. The instability is accompanied by non-uniqueness of flow regimes in certain bands of M_∞ and α. In particular, there exist two symmetric (about the x-axis) and two asymmetric steady flows at $\alpha=0$, $1.77 \leq M_\infty \leq 1.91$ for the centerbody thickness $T=0.12$. An increase of the centerbody length enlarges the hysteresis band. Computations of the 3D flow confirmed the existence of axisymmetric regimes at the vanishing angle of attack, though demonstrated an impact of the sidewall on Mach number distributions in spanwise sections z=const.
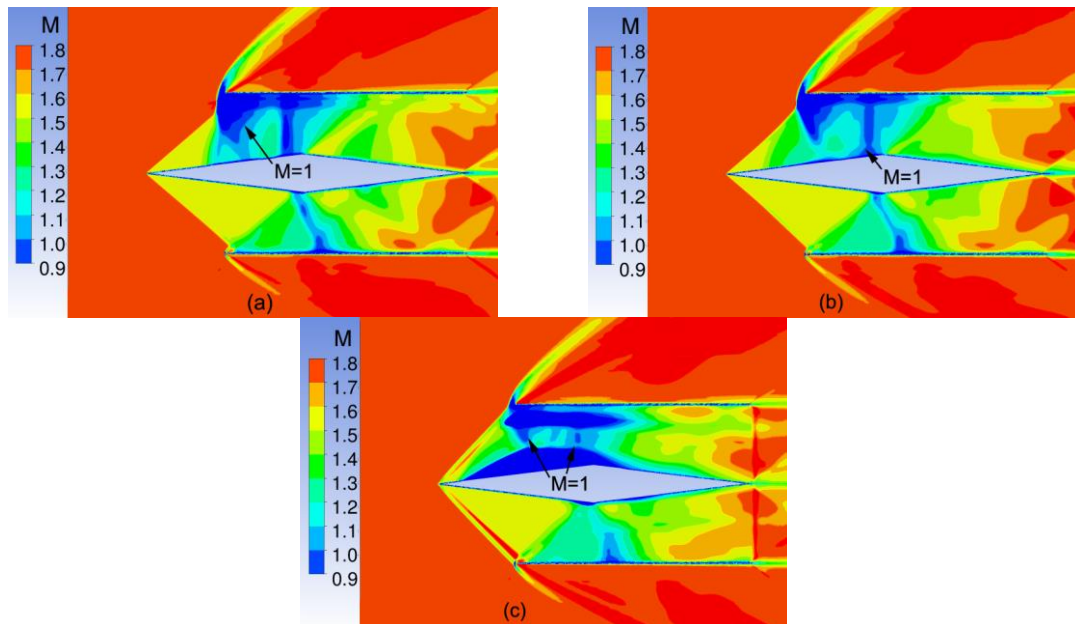
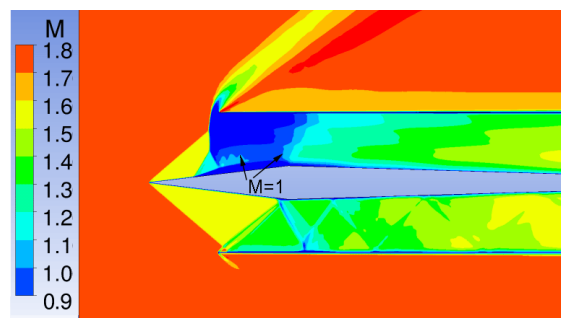Fig. 12 Mach number contours in span sections of the 3D flow shown in Fig. 11: (a) *z*=0, (b) *z*=0.075, (c) *z*=0.14

Fig. 13 Mach number contours in 2D flow over the longer centerbody. The same asymmetric flow regime at M_∞=1.8, α=0 as in Fig. 5
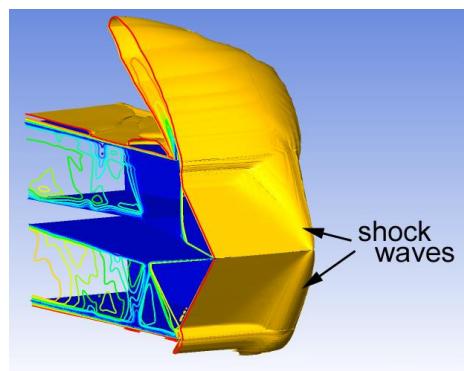

Fig. 14 Mach number contours in the plane *z*=0 and isosurfaces *M*(*x*, *y*, *z*)=1.7 in/over a longer channel of half-span 0<*z*<0.3. The same asymmetric flow regime at M_∞=1.8, α=0 as in Fig. 5

Acknowledgments

References

Военное обозрение (2018), Ту-160. Стоит ли возобновлять производство?; Военное обозрение, Russia, https://topwar.ru/138306-tu-160-stoit-li-vozobnovlyat-proizvodstvo.html.

Barth, T. and Jespersen, D. (1989), "The design and application of upwind schemes on unstructured meshes", AIAA PAPER 89-0366; NASA Ames Research Center, CA, U.S.A.

Ben-Dor, G. (2007), *Shock Wave Reflection Phenomena*, Springer, Berlin, Germany.

Ben-Dor, G. (2015), "Hysteresis phenomena in reflection of shock waves", *29th International Symposium on Shock Waves 1*, Springer, Berlin, Germany.

Chang, J., Li, N., Xu, K., Bao, W. and Yu, D. (2017), "Recent research progress on unstart mechanism, detection and control of hypersonic inlet", *Progress Aerosp. Sci.*, **89**, 1-22.

Chang, J., Yu, D., Bao, W., Fan, Y. and Shen, Y. (2009), "Effects of boundary-layers bleeding on unstart/restart characteristics of hypersonic inlets", *Aeronautical J.*, **113**(1143), 319-327.

Daneshyar, H. (1976), *One-dimensional Compressible Flow: Thermodynamics and Fluid Mechanics Series*, Pergamon, Oxford, United Kingdom.

Das, S. and Prasad, J.K. (2010), "Starting characteristics of a rectangular supersonic air-intake with cowl deflection", *Aeronautical J.*, **114**(1153), 177-189.

Hill, P. and Peterson, C. (1992), *Mechanics and Thermodynamics of Propulsion Systems*, *2nd Ed.*, Addison-Wesley Pub. Ltd., London, United Kingdom.

Hu, R., Jameson, A. and Wang, Q. (2011), "Adjoint based aerodynamic optimization of supersonic biplane airfoils", AIAA paper 2011-1248; *49th AIAA Aerospace Sciences Meeting including the New Horizons Forum and Aerospace Exposition*, Florida, U.S.A., January.

Jiao, X., Chang, J., Wang, Z. and Yu, D. (2015), "Mechanism study on local unstart of hypersonic inlet at high Mach number", *AIAA J.*, **53**(10), 3102-3112.

Jiao, X., Chang, J., Wang, Z. and Yu, D. (2016), "Hysteresis phenomenon of hypersonic inlet at high Mach number", *Acta Astronautica*, **128**, 657-668.

Kantrowitz, A. and Donaldson, C. (1945), "Preliminary investigation of supersonic diffusers", NACA-ACR-L5D20; National Advisory Committee for Aeronautics, Langley Memorial Aeronautical Laboratory, U.S.A.

Kusunose, K., Matsushima, K. and Maruyama, D. (2011), "Supersonic biplane – A review", *Progress Aerosp. Sci.*, **47**(1), 53-87.

Kuzmin, A. (2014), "On the lambda-shock formation on ONERA M6 wing", *J. App. Eng. Res.*, **9**(20), 7029-7038.

Kuzmin, A. (2015), "Shock wave instability in a channel with an expansion corner", *J. App. Mech.*, **7**(2), 1-9.

Kuzmin, A. (2016), "Shock wave bifurcation in convergent – divergent channels of rectangular cross section", *Shock Waves*, **26**(6), 741-747.

Kuzmin, A. and Babarykin, K. (2016), "Transonic flow bifurcation in symmetric channels with centerbodies", *Estestvennye i matematicheskie nauki v sovremennom mire*, **10**(45), SibAc Publishing House, Novosibirsk, Russia.

Li, Z., Huang, B. and Yang, J. (2011), "A novel test of starting characteristics of hypersonic inlets in shock tunnel", *17th AIAA International Space Planes and Hypersonic Systems and Technologies Conference*, California, U.S.A., April.

Menter, F.R. (2009), "Review of the shear-stress transport turbulence model experience from an industrial

perspective", *J. Comp. Fluid Dyn.*, **23**(4), 305-316.

Mölder, S. and Timofeev, E. (2011), "Hypersonic air intake design for high performance and starting", *RTO - Educational Notes Paper*, RTO-EN-AVT-195; NATO STO, Italy.

Nguyen, T., Behr, M., Reinartz, B.U., Hohn, O. and Gülhan, A. (2011), "Numerical investigations of the effects of sidewall compression and relaminarization in 3D scramjet inlet", *17th AIAA International Space Planes and Hypersonic Systems and Technologies Conference*, California, April.

Riabinin, A. and Suleymanov, A. (2016), "Bifurcation of transonic flow in the channel with a central body", *Proceedings of Conference Topical Problems of Fluid Mechanics 2016*, Prague, Czech Republic, April.

Sforza, P.M. (2012), *Theory of Aerospace Propulsion*, Academic Press, MA, U.S.A.

Tao, C., Daren, Y., Juntao, C. and Wen, B. (2008), "Topological geometry interpretation of supersonic inlet start/unstart based on catastrophe theory", *J. Aircraft*, **45**(4), 1464-1468.

Tao, C., Daren, Y., Juntao, C. and Wen, B. (2009), "Catastrophe model for supersonic inlet start/unstart", *J. Aircraft*, **46**(4), 1160-1166.

Timofeev, E. and Mölder, S. (2011), "Supplemental Notes to the Lecture 'Theoretical Analysis of Flow Starting in Hypersonic Airntakes with CFD Illustrations'", EN-AVT-195-07-Suppl; NATO STO, Italy.

Wikipedia (2017), North American XB-70 Valkyrie; Wikipedia, en.wikipedia.org/wiki/North_American_XB-70_Valkyrie.

Xu, K., Chang, J., Zhou, W. and Yu, D. (2016), "Mechanism and prediction for occurrence of shock-train sharp forward movement", *AIAA J.*, **54**(4), 1403-1412.

Yamashita, H., Kuratani, N., Yonezawa, M., Ogawa, T., Nagai, H., Asai, K. and Obayashi, S. (2013), "Wind tunnel testing on start/unstart characteristics of finite supersonic biplane wing", *J. Aerosp. Eng.*, **2013**, 1-10.

EC